



# Minor element effect on high temperature corrosion of a low-alloyed steel: Insight into alkali- and chlorine induced corrosion by means of atom probe tomography

A. Persdotter<sup>a,\*</sup>, T. Boll<sup>b,c</sup>, T. Jonsson<sup>a</sup>

<sup>a</sup> Division of Energy and Materials, Chalmers University of Technology, SE-412 96 Sweden

<sup>b</sup> Institute for Applied Materials (IAM-WK), Karlsruhe Institute of Technology (KIT), Engelbert-Arnold-Str. 4, D-76131 Karlsruhe, Germany

<sup>c</sup> Karlsruhe Nano Micro Facility (KNMF), Karlsruhe Institute of Technology (KIT), Hermann-von-Helmholtz-Platz 1, D-76344 Eggenstein-Leopoldshafen, Germany

## ARTICLE INFO

### Keywords:

High temperature corrosion  
Low-alloy steel  
Chlorine  
Alkali  
Transmission electron microscopy  
Atom probe tomography

## ABSTRACT

High temperature corrosion remains a challenge for many high temperature applications. The corrosion resistance may be improved by the addition of minor amounts of reactive alloying elements. However, in the presence of corrosive species, such as alkali and chlorine, the corrosion rates are often highly accelerated. This study implements STEM/EDX and APT in order to shed light on a possible destructive minor element effect by investigating how the presence of minor amounts of corrosive species in the iron oxide formed on a low-alloyed steel may impair the corrosion resistance by increasing the oxide growth rate and possibly also reduce the oxide integrity.

## 1. Introduction

Many high temperature applications suffer from high temperature corrosion. The corrosion resistance of high temperature materials rely on the formation of a protective, i.e. slow-growing and well-adherent, oxide scale. The protection of high alloyed steels often consist of Cr and/or Al-rich  $M_2O_3$  oxide scales, whereas low-alloyed Fe-base alloys form multi-layered Fe-rich oxide scales composed of an outward-growing duplex iron-oxide scale ( $Fe_2O_3$  on top of  $Fe_3O_4$ ) and an inward-growing mixed spinel ( $(Fe,Cr,M)_3O_4$ ) [1,2]. The Cr/Al-type of scale is used as protection at higher temperatures while the Fe-rich oxide is often sufficient at lower/moderate temperatures, such as at the 400 °C investigated in this study.

It is well known that minor amounts ( $\leq 1\%$ ) of reactive alloying elements (e.g. Y, La, Ce, Zr, Hf) improve the protective properties of both Cr- and Al-rich  $M_2O_3$  oxide scales, decreasing corrosion e.g. by reducing the oxide growth rate and/or increasing the scale/metal adhesion [3–6, 7]. This effect is known as the reactive element effect (REE) and has been studied extensively (see e.g. reviews by Whittle and Stringer 1980 [3] and Naumenko 2016 [6]). The information on oxide microstructure and chemistry has been shown to be very important in order to better understand the reactive element effect on high temperature corrosion. In order to study the influence of reactive elements in detail and detect the

distribution of the small amounts present in oxide scales, advanced analysis methods are required such as e.g. Atom probe tomography (APT) or High resolution transmission electron microscopy (HR-TEM) in combination with Energy dispersive X-ray spectroscopy (EDS) or Energy loss spectroscopy (EELS) [8–10].

In contrast to the beneficial effects of reactive elements, accelerated corrosion may be observed when minor amounts of corrosive species, such as e.g. chlorine and alkali, from the environment are present in the oxide scale. The influence of alkali and chlorine containing species on high temperature corrosion has been extensively studied on both stainless- and low-alloyed steels [11–38]. Even though it is well known that chlorine- and alkali containing species tend to accelerate corrosion of all these materials, the underlying mechanisms of both chlorine and alkali containing species are still under debate. For stainless steels, previous studies have shown that alkali (potassium in particular) may influence corrosion by the depletion of Cr from the protective Cr-rich corundum type oxide. This results in breakaway corrosion and the formation of a less protective iron-rich oxide scale [22–25,26]. However, low-alloyed steels form the iron-rich type of oxide scale both in the presence and absence of alkali and chlorine. Thus, the origin for the well-observed influence of alkali and chlorine on low-alloyed steels remains uncertain.

Different theories have been proposed to explain the effects, often

\* Corresponding author.

E-mail address: [amanda.persdotter@chalmers.se](mailto:amanda.persdotter@chalmers.se) (A. Persdotter).

<https://doi.org/10.1016/j.corsci.2021.109779>

Received 8 April 2021; Received in revised form 14 August 2021; Accepted 15 August 2021

Available online 6 September 2021

0010-938X/© 2021 The Author(s). Published by Elsevier Ltd. This is an open access article under the CC BY license (<http://creativecommons.org/licenses/by/4.0/>).

focused on the influence of chlorine. One mechanism, initially proposed by McNallan et al. [39] and further developed by Grabke et al. [13] is through active oxidation (i.e. the chlorine cycle), which has been suggested in a wide temperature and material range [11,13–16,18,19,21,27,39]. The theory is based on a cyclic process where chlorine is suggested to act as a catalyst for oxide growth by the formation of volatile metal chlorides that evaporate and decompose to  $\text{Cl}_2$  and iron-oxide, forming porous outward-growing oxides. Folkesson et al. [35] studied the low-alloyed steel Fe2.25Cr1Mo and suggested that the accelerated oxide growth observed in the presence of KCl (at 400 and 500 °C) was attributed to a mechanism referred to as the electrochemical mechanism. The mechanism suggested KCl to react and form potassium hydroxide and release  $\text{Cl}^-$  ions, that in turn could form iron chlorides. The iron chlorides were suggested to decorate oxide grain boundaries, facilitating grain boundary transport of both iron and oxygen through the oxide scale.

Several previous studies have observed accelerated corrosion of low-alloyed steels also when no, or very small amounts (around the detection limit of the performed analysis), of these elements are detected in the formed oxide scale [33,35,37], making it difficult to conclude the actual role of alkali and chlorine. Thus, one may speculate that the accelerated corrosion observed on low-alloyed steels in the presence of corrosive species, such as chlorine and alkali, may be a parallel effect, a minor element effect, to the reactive element effect, by the reduction (instead of improvement) of the protective properties of the formed oxide scale. In order to investigate this and increase the understanding of why potassium and chlorine may reduce the corrosion protection of low-alloyed steels, more advanced analytical tools, with lower chemical detection limits as well as higher spatial resolution, are required.

The aim of this study is to investigate the low-alloyed steel Fe2.25Cr1Mo, by detailed characterization of the distribution of potassium and chlorine in the multi-layered Fe-oxide scale formed at 400 °C, by means of Atom probe tomography (APT). The results will be linked to the STEM/EDX results and oxidation kinetics. This is in order to gain insight into why minor amounts of these species may accelerate the corrosion in high temperature applications, such as observed e.g. in biomass and waste-fired boilers [40–43].

## 2. Experimental procedure

### 2.1. Exposures and sample preparation

The composition of the investigated steel, Fe-2.25Cr-1Mo, is shown in Table 1. Prior to exposure the steel was cut into coupons ( $15 \times 15 \times 2$  mm), ground with SiC (P4000), a Largo disc (9  $\mu\text{m}$ ) and polished with diamond suspension (3 and 1  $\mu\text{m}$ ) until mirror like appearance. The polished coupons were degreased and cleaned in acetone and ethanol by using ultrasonic agitation. The influence of alkali and chlorine was investigated by deposition of 0.1  $\text{mg}/\text{cm}^2$  KCl(s) onto the steel surface prior to exposure. The deposition of KCl(s) was performed by spraying a solution of KCl solved in ethanol and water (80:20) and subsequently dried in cool air.

The steel coupons used for microstructural analysis were exposed in an isothermal horizontal tube furnace in 20%  $\text{H}_2\text{O} + 5\% \text{O}_2 + 75\% \text{N}_2$  at 400 °C for 24 h. The conditions are chosen to mimic a simplified environment in a biomass- and/or waste fired boiler. The samples were positioned parallel to the direction of the gas flow and all parts of the systems were kept above the dew point of water to prevent condensation. All samples were stored in a desiccator prior to exposure and awaiting analysis to avoid atmospheric corrosion and minimize

hygroscopic effects of chlorine containing species. However, hygroscopic effects of chlorine containing species are still expected due to handling in air between analysis as well as time of storage. Thermogravimetric analysis (TGA) was performed, with and without KCl(s) deposited onto the sample, in order to observe how the presence of KCl (s) influences the oxidation kinetics. The TGA was conducted by using a Setaram Setsys thermobalance (flow rate of 15 ml/min) humidified with a Setaram Wetsys (for more details see [37]).

Site specific cross sections for TEM analysis and APT measurements were prepared using an FEI Versa3D LoVac DualBeam and a FEI Strata, respectively. The instruments were operated in high vacuum mode at 30 keV, with varying beam currents (30 pA - 15 nA) throughout the lift-out procedure. The representability of the TEM and APT samples were ensured by SEM investigation, as well as previous microstructural investigation performed by Persdotter et al. [37].

### 2.2. Analytical techniques

The oxide scale was investigated by means of Scanning electron microscopy (SEM), Transmission electron microscopy (TEM) and Atom probe tomography (APT). A plan-view SEM investigation was performed to choose representative regions for detailed characterization by means of TEM and APT. The instruments used were a Zeiss LEO Ultra 55 FEG SEM and an FEI Quanta ESEM 200 operated in high vacuum at 10–20 keV.

The oxide scale microstructure and composition was investigated in cross section using an FEI Titan 80–300 TEM equipped with an Oxford X-sight EDX detector for chemical analysis. The microscope was operated in Scanning TEM mode (STEM), at an accelerating voltage of 300 keV. Both bright field (BF) and High Angle Annular Dark field (HAADF) imaging modes were used. Due to large errors associated with oxygen quantification in EDX analysis cationic percent are reported (in at%), assuming stoichiometric oxides.

The APT measurements were performed on a Cameca Local Electrode Atom Probe (LEAP 4000X HR) at a set temperature of 60 K, a laser pulse energy of 30 pJ, an evaporation frequency of 100–200 kHz and a detection rate of 0.3%. The 3D atom maps were reconstructed based on SEM images and evaluated with IVAS 3.6.14. As for the EDX analysis, oxygen is excluded in the reported quantification, if not stated otherwise.

## 3. Results

### 3.1. Oxidation kinetics

The oxidation kinetics of Fe2.25Cr1Mo in exposure to 5%  $\text{O}_2 + 20\% \text{H}_2\text{O} + 75\% \text{N}_2$  in the absence and presence of 0.1  $\text{mg}/\text{cm}^2$  KCl(s) is shown in Fig. 1. It is evident that the small amounts of KCl highly accelerate the oxide growth rate. The growth is parabolic both in the absence and presence of KCl, with a parabolic rate constant orders of magnitude lower in the absence ( $k_{p,\text{Ref}} \sim 10^{-14} \text{ g}^2 \text{ cm}^{-4} \text{ s}^{-1}$ ) compared to in the presence of KCl ( $k_{p,\text{KCl}} \sim 10^{-12} \text{ g}^2 \text{ cm}^{-4} \text{ s}^{-1}$ ). The parabolic rate constants,  $k_p$ , were calculated from  $\Delta m^2 = 2k_p t$ , where  $\Delta m$  represent the mass change (y-axis) and  $t = \text{time}$  (x-axis).

Persdotter et al. [37] showed that longer exposure times (24 h) in the same exposure environment included a kinetic transition suggested to be explained by oxide delamination, followed by crack formation of the oxide scale. The oxide growth remained parabolic, with similar parabolic rate constants, both before and after the kinetic transition (i.e. delamination). Thus, the first formed oxide scale (formed before the

**Table 1**  
Nominal composition (wt%) of Fe-2.25Cr-1Mo [50].

Fe	Cr	Mo	Mn	Si	C	P	S
Bal.	1.9–2.6	0.87–1.13	0.3–0.6	$\leq 0.50$	0.05–0.15	$< 0.025$	$< 0.025$

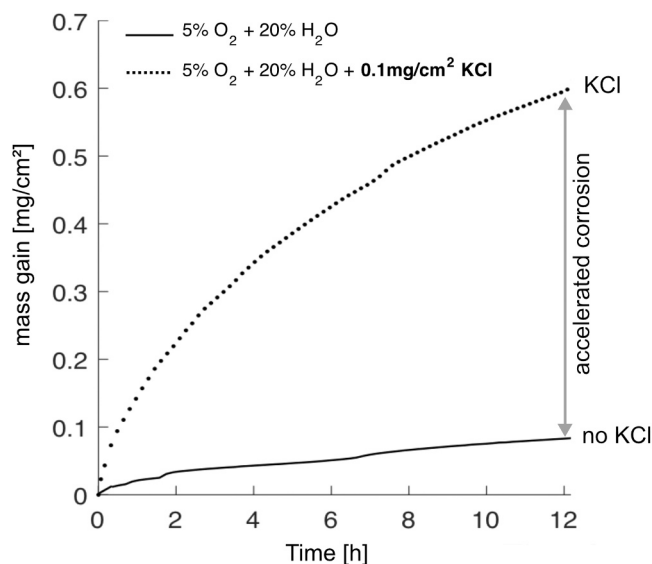


**Fig. 1.** Mass gain data (first 12 h) for Fe-2.25Cr-1Mo exposed in a thermobalance in 5% O<sub>2</sub> + 20% H<sub>2</sub>O + 75% N<sub>2</sub> at 400 °C in the presence and absence of KCl(s).

delamination, ≤ 12 hrs) is therefore used in this study to analyze the influence of small amounts of KCl in further detail, representing a typical oxide scale grown on Fe<sub>2.25</sub>Cr<sub>1</sub>Mo under these exposure conditions.

### 3.2. Oxide scale microstructure and composition

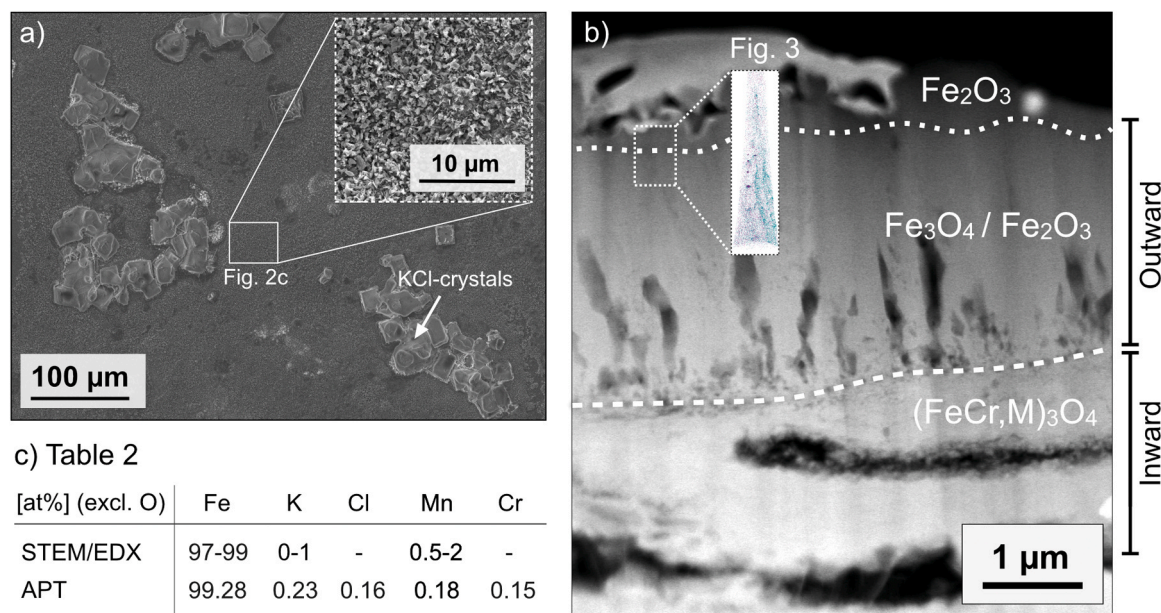
The oxide microstructure of Fe<sub>2</sub>-25Cr<sub>1</sub>Mo exposed for 24 h in the reference exposure (no KCl, 5% O<sub>2</sub> + 20% H<sub>2</sub>O + 75% N<sub>2</sub> at 400 °C) has been investigated in detail in a previous study [37]. The oxide scale is approximately 0.5 μm thick and consists of an outward-growing iron oxide (0.13 μm Fe<sub>2</sub>O<sub>3</sub> on top of 0.26 μm Fe<sub>3</sub>O<sub>4</sub>) and a 0.13 μm inward-growing mixed spinel oxide ((Fe,Cr,M)<sub>3</sub>O<sub>4</sub>).

Fig. 2a shows a plan view image of the oxide scale formed on

Fe<sub>2</sub>-25Cr<sub>1</sub>Mo exposed for 24 h in 5% O<sub>2</sub> + 20% H<sub>2</sub>O + 75% N<sub>2</sub> at 400 °C in the presence of KCl(s). The region of interest in this study is the base oxide (in between remaining KCl-crystals) as marked in Fig. 2a, showing a granular oxide morphology (see inserted figure). This type of oxide covers approximately 80% of the sample surface and is suggested to be the main contributor to the accelerated mass gain observed. No, or very limited amounts, of KCl was deposited in these regions prior to exposure, but were expected to spread rapidly over the sample surface during exposure [34]. The STEM-HAADF image shown in Fig. 2c shows the oxide cross section from this region (top part, ≤ 12 h). The oxide scale is multi-layered, in similarity to the reference sample, consisting of an outward-growing iron oxide and an inward-growing mixed spinel oxide. The oxide grains in the outward-growing Fe<sub>3</sub>O<sub>4</sub> are columnar with a measured oxide grain width ranging from 60 to 300 nm.

The oxide composition of the outward-growing oxide, as detected by STEM/EDX analysis, is shown in Table 2 in Fig. 2c. The atomic composition (oxygen excluded), indicated that the outward-growing oxide is a rather pure iron oxide (97–99 at%), that contained approximately 0.5–2 at% Mn and 0–1 at% K. No chlorine signal was detected by STEM/EDX in this oxide layer. It should be noted that the exact amount of Mn is challenging to quantify due to overlapping peaks with iron. However, qualitatively it is evident, from the STEM/EDX spectrum, that Mn and K were present in the iron oxide scale. Note that the local distribution of Mn and K remained unknown from these measurements and that the detection limit of STEM/EDX limits the amount of trace elements that could be detected. Thus, from these results it is still possible that trace amounts of Cl is included in the oxide layer. It may also be noted that the oxide scale suggested to form after the kinetic transition (after 12 h, not shown) also contained trace amounts of K (approximately 0.5 at% K).

In order to investigate the indications of small amounts of K, Mn and study possible trace amounts of Cl in the iron oxide, APT was employed. A representative region of the iron oxide was selected, i.e. the top part of the outward-growing oxide. The region of interest (ROI) for the APT measurements is indicated in Fig. 2b. The overall bulk composition of the APT-tip, as measured by APT, is shown in Table 2 in Fig. 2c (oxygen excluded). Oxygen is excluded due to challenges associated with oxygen quantification in APT. The amount of oxygen was quantified to 50.56 at%



**Fig. 2.** The top part of the oxide scale (suggested to form during the first 12 hrs) formed on Fe-2.25Cr-1Mo exposed for 24 h in 5% O<sub>2</sub> + 20% H<sub>2</sub>O + 75% N<sub>2</sub> at 400 °C in the presence of KCl(s). The SEM-SE images (a) shows the base oxide (in between remaining KCl-crystals) while the STEM-HAADF (b) image shows the cross section and region of interest for APT measurements. (c) shows the composition (oxygen excluded) of the outward-growing oxide as detected by STEM/EDX and APT (the bulk composition of the APT-tip).



%, which is much lower than expected for an  $\text{Fe}_2\text{O}_3/\text{Fe}_3\text{O}_4$  oxide scale. Thus, only the atomic percentages, excluding oxygen, are shown in Table 2 (see Fig. 2c).

Fig. 3a shows the distribution of potassium and chlorine in the top iron oxide from one representative APT-measurement. The atom map (Fig. 3a) clearly shows that potassium atoms are segregated to regions interpreted to be oxide grain boundaries. The size of the APT-tip agrees well with the smaller grains ( $\sim 75$  nm) observed by STEM imaging in this oxide (not shown, see [37] for more details). Thus, it is probable to capture oxide grains within a randomly chosen APT-tip from this region, as observed in this study. It is evident that the segregation of potassium at the grain boundaries is accompanied by the presence of small clusters of KCl (diameter up to  $\sim 5$  nm) in the iron-oxide scale (not specifically at the grain boundaries). The trace amounts of Cl that appear to be distributed homogeneously throughout the APT-tip (Fig. 3a) are caused by overlapping peaks with FeO/FeOH in the m/q-spectrum (see Fig. 4b) and should be neglected. Thus, the trace amounts of Cl detected by APT ( $\leq 0.2$  at%) throughout the tip can be neglected and the interpretation is that no Cl is present in the oxide grain boundaries or in the bulk oxide,

but could only be found in the KCl-nanoclusters. It should be noted, however, that the high oxygen partial pressure present in the top part of the oxide scale would result in oxidation of metal chlorides if formed (thus not detectable).

Fig. 3b-c shows 1D-concentration profiles over the KCl nanoclusters (Fig. 3b) as well as K-segregated grain boundaries (Fig. 3c) (see markings for regions and profile direction in Fig. 3a). The clusters contain up to approximately 12 at% K and 7 at% Cl (see Fig. 3b), excluding oxygen in the quantification (Fe in balance:  $\sim 81$  at%). The main elements oxygen ( $\sim 45$  at% O) and iron ( $\sim 45$  at% Fe) were detected, since the clusters lay within an iron oxide. The nanoclusters are, however, interpreted to be pure KCl clusters, with a K:Cl ratio of approximately 12:7, which is likely to be slightly overestimated due to troublesome overlaps at 37 Da (see Fig. 4b), resulting in that only the peak at 35 Da is included for the quantification of Cl.

Fig. 3c shows a 1-D concentration profile across an oxide grain boundary (see marking for region in Fig. 3a), showing that the grain boundary contains up to approximately 2.3 at% K (excluding oxygen in the quantification). Small amounts of Mn ( $\leq 0.4$  at% Mn) were also

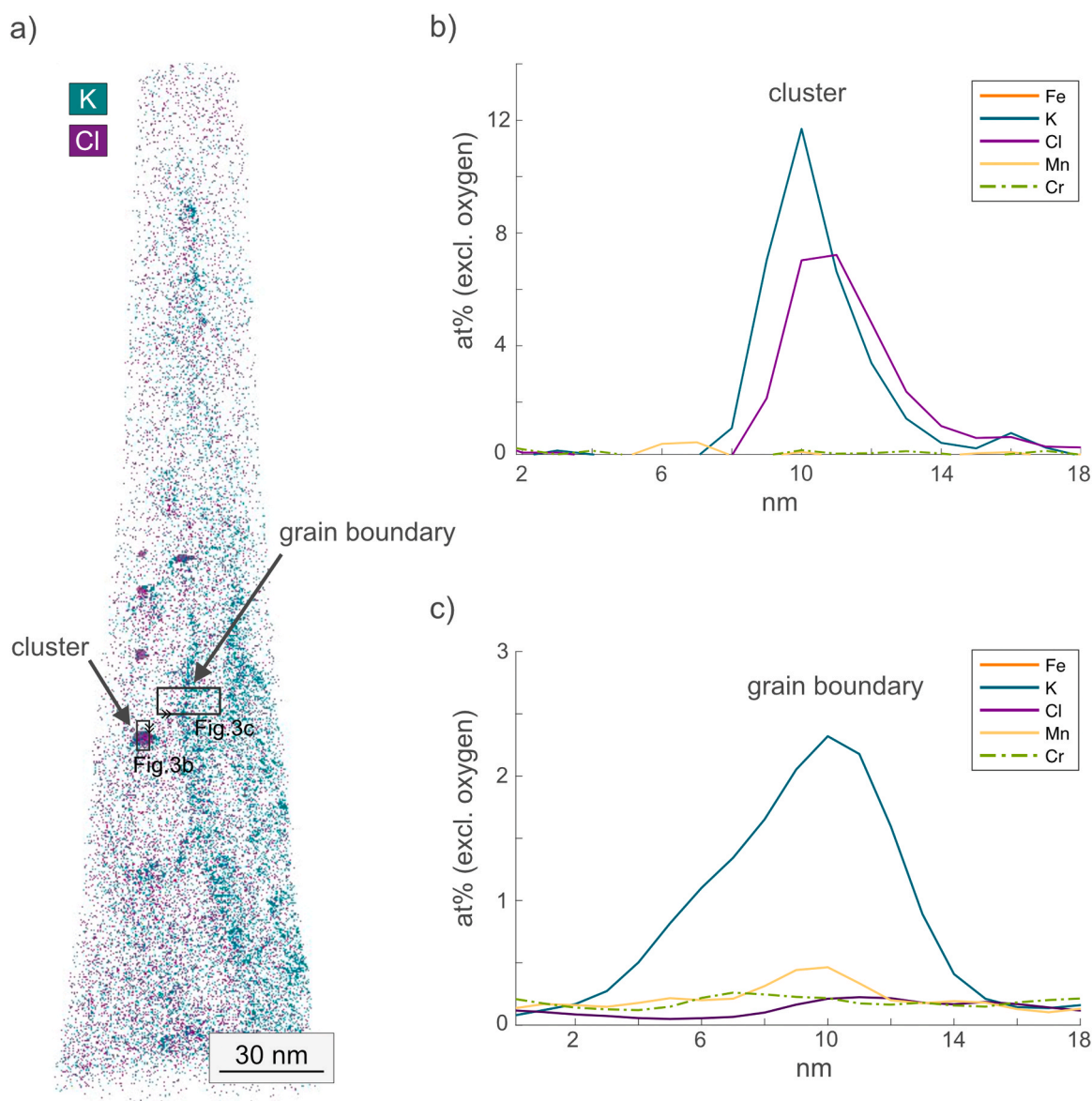
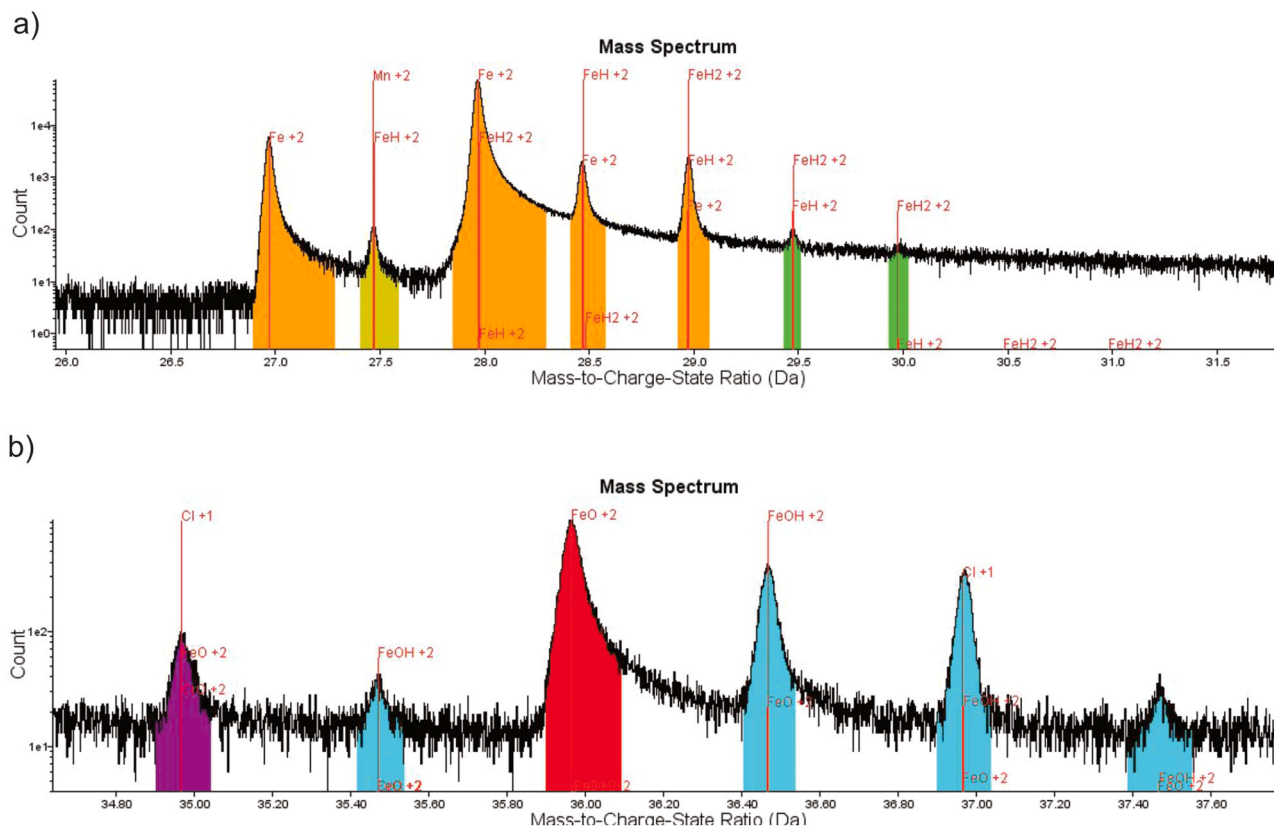


Fig. 3. APT results from the top of the outward-growing oxide scale grown on Fe-2.25Cr-1Mo exposed in 5% $\text{O}_2$  + 20% $\text{H}_2\text{O}$  + 75% $\text{N}_2$  at 400 °C for 24 h in the presence of KCl(s). (a) Atom map of a representative APT measurement, (b-c) 1-D concentration profiles (excluding oxygen) over regions marked in 3a (clusters(b) and segregation to oxide grain boundaries(c)).



**Fig. 4.** Mass-to-charge spectrum showing troublesome overlaps. a) Between 27 and 30 Da the Fe, FeH<sub>x</sub> and Mn overlaps with several KOH/KO peaks. b) Cl-peaks at 35 and 37 Da overlaps with both FeO and FeOH.

indicated to segregate to oxide grain boundaries while trace amounts of Cl ( $\leq 0.2$  at%) and Cr ( $\leq 0.2$  at%) as well as the main element Fe ( $\sim 81$  at%, excluding oxygen) were homogeneously distributed in this region. The main elements oxygen (up to  $\sim 47.5$  at% O) and iron (up to  $\sim 50.5$  at% Fe) were also detected since the potassium segregation to the oxide grain boundaries occurs within an iron oxide scale. As mentioned above, the trace amounts of Cl detected homogeneously throughout the APT-tip should be neglected due to overlapping peaks with FeO/FeOH in the m/q-spectrum (see Fig. 4b). Thus, the interpretation is that only K, and indications of Mn, are segregated to the oxide grain boundaries. It should be noted that the potassium accumulates also to the surroundings of the oxide grain boundaries, as can be seen by the relatively wide distribution of potassium (several nanometers) around the oxide grain boundary in Fig. 3c. Note also that the distribution is slightly asymmetric. The asymmetry could possibly be explained by that the 1D-concentration profile is cut from a 3D-volume and the difficulty to capture the often not straight profile exactly perpendicular to a grain boundary. However it could also be that the bulk-diffusion of K into the grains on either side of the boundary varies due to e.g. the orientation or doping. The asymmetric distribution would need more investigation in order to explain with any certainty.

As briefly mentioned above, a few challenging overlaps could be distinguished in the mass-to-charge (m/q) spectrum, that makes it difficult to quantify the bulk composition and the 1D-concentration profiles (see Fig. 4). One example is the Fe, FeH and FeH<sub>2</sub> that have several overlaps with KOH (Fig. 4a). However, from analyzing the spectrum and the homogeneous distribution of atoms from these peaks, the interpretation is that KOH is not the main contributor to the overlapping peak, but that these peaks originate from Fe and its hydrides. Due to the commonly observed diffusion of hydrogen during APT-measurements, it is not possible to say whether the hydrides are part of the thermally grown oxide or if they have formed during the APT-

measurement. Another challenging overlap, shown in Fig. 4a, is the peak at around 27 Da. The main contributor to this peak is concluded to be Mn, and the results indicate that it segregates to the oxide grain boundaries (not shown). However, the concentration is not certain, due to overlaps with FeH, and conclusions regarding this segregation should be made with care. Fig. 4b also shows challenging overlaps of Cl-peaks at 35 and 37 Da with both FeO and FeOH. This is suggested to explain the homogeneous distributed Cl-signal observed in Fig. 3a. In addition, small amounts of CrO<sub>3</sub> and FeO<sub>3</sub> were detected homogeneously distributed in the APT tip. One peak of CrO<sub>3</sub> and FeO<sub>3</sub> is overlapping, resulting in the possibility of that Cr is slightly overestimated.

## 4. Discussion

### 4.1. General observations

As many previous studies have shown, the presence of KCl accelerates the oxide growth rate on low-alloyed steels [15,33–37], in good agreement with the results from this study. The oxidation kinetics presented in this study is parabolic both in the absence and presence of KCl, in good agreement with previous studies [35–37], suggesting that the growth is diffusion controlled in both exposure environments. The parabolic rate constant,  $k_p$ , is observed to be nearly two orders of magnitude higher in the presence of KCl, indicating that the diffusion properties of the oxide scale change in the presence of KCl, even though very small amounts of KCl are present, see Fig. 1. However, from the oxidation kinetics, it is not obvious whether it is the bulk or grain boundary diffusion that has been altered, compared to exposure in the absence of KCl. The microstructural investigation focuses on a region with very little KCl present. Previous studies by Persdotter et al. [37] showed that the growth rate of both the inward-growing scale (i.e. diffusion of oxygen) as well as the outward-growing scale (i.e. diffusion

of iron) increased in this region in exposure to KCl, even more so for the inward-growing scale. It may also be noted that this environment increased the tendency for scale delamination and cracking after longer exposures [37]. It is well known that grain boundary diffusion is an important aspect for the oxidation kinetics of iron oxides in this temperature range [2]. Thus, the focus of the investigation was mainly confined to grain boundaries in the oxide scale.

#### 4.2. Minor element effect - segregation of K/Cl/Mn

The addition of minor amounts of certain reactive alloying elements (Y, La, Ce, Zr, Hf etc.) is well known to improve both oxide growth rates and/or adhesion [3,6]. The reactive element effect is normally easy to detect in oxidation kinetics while the presence of reactive elements in the oxide scale may be more challenging to show. Reactive elements have been found in very low levels at grain boundaries/interfaces, but still give rise to large effects on oxidation kinetics [6,44]. It may be speculated that certain other elements could have a similar, but destructive effect on oxidation kinetics. APT is a very useful tool in order to track small amounts of elements to better understand the mechanisms. This study implements APT in order to investigate how the presence of minor amounts of corrosive species (e.g. K and Cl) in the iron oxide scale formed on a low-alloyed steel may impair the corrosion resistance by increasing the oxide growth rate and possibly also reducing the oxide integrity.

The STEM/EDX and especially the APT results indicate that the presence of small amounts of potassium has influenced the chemistry of the outward-growing iron oxide. The APT results suggest that potassium is segregated to oxide grain boundaries, accompanied with small nanoclusters of potassium chloride (KCl) distributed throughout the outward-growing oxide (see Fig. 3). The K segregation to oxide grain boundaries may possibly be part in explaining both the accelerated diffusion observed, by influencing the diffusion rate along grain boundaries, and the oxide cracking observed in the presence of KCl(s), by changing the mechanical properties of the oxide scale to make it more brittle. From the results in this study it cannot be concluded what phase the detected potassium is bound to. Previous studies have suggested reactions resulting in the formation of  $KFeO_2$  [38,45] or KOH [35] in exposure to KCl. However, these phases could not be detected in this study. KOH was indicated in the m/q spectrum from the APT measurements, but due to overlaps it could not be concluded with certainty. The grain boundary segregation of potassium is not accompanied by chlorine or any other elements apart from indications of trace amounts of Mn. It is well known that Mn may diffuse fast through a spinel oxide, especially at higher temperatures [46]. Thus, the presence of Mn at the grain boundaries could simply be an effect of a higher diffusion rate in these regions, compared to the bulk. This would mean that it is only a matter of time before Mn would spread also to the bulk oxide.

The oxide grain boundary segregation of K is relatively wide (~ 10 nm), in agreement with several previous APT studies on oxide grain boundaries [8,10,47]. For reference, a grain boundary is often considered to be approximately 0.5 nm [48]. The wide distribution indicates that potassium influences the grain boundary as well as the surroundings of the oxide grain boundaries, by widening the region of disorder between the oxide grains. A larger (i.e. wider) disordered region may explain the increase in total diffusion rate observed by the creation of larger short circuit diffusion paths for both iron, oxygen as well as other species, such as chlorine, through the scale. These results, in combination with the observations of more inward-growing scale, as compared to outward-growing scale in the presence of KCl, indicate that this effect is mainly on the anion diffusion, i.e. of oxygen and chlorine. It should be noted that even though no accumulation of Cl was observed at the grain boundary regions, this does not rule out the grain boundaries as diffusion paths for Cl, as Cl may have reacted and/or migrated from the grain boundary regions during the ramping down in temperature and after exposure.

#### 4.3. Minor element effect – mechanisms

The accelerated corrosion rate, associated with K segregation to oxide grain boundaries may shed some light on previous investigations/mechanisms where the chemical analysis often show no, or indicate very small amounts, of these species in the oxide scale after exposure [15, 33–37]. The near absence of these species in a large part of the traditional analysis has made it difficult to explain how they interact with the oxide scale to accelerate the overall corrosion rate. Nevertheless, several theories have been suggested to explain the obvious influence observed, such as e.g. the chlorine cycle [13,39], formation of metal chlorides at the oxide grain boundaries and alkaline conditions (KOH) at the scale/gas interface [35,36], as well as eutectic melt formation ( $KCl-FeCl_2$ ) and proposed chlorine decoration of oxide grain boundaries [34]. The present results indicate a change in microstructure, possibly increasing the diffusion, through a wider disordered region between oxide grains. An increased overall diffusion rate through these disordered regions could result in a faster diffusion of both oxygen and Cl ions through the scale. This would explain the increased amount of inward-growing, as compared to outward-growing, scale observed in exposure to KCl. However, no Cl could be detected in the analysis. A possible explanation to how the potassium segregation may accelerate the growth rate of iron oxide scales could also be if the widened grain boundary regions would act as a type of micro cracks where the potassium could be present in the form of a melt (the  $KCl-FeCl_2$  system forms a eutectic at 355 °C [34]). Diffusion, of both oxygen, iron and other species, through a melt is known to be fast, in comparison to both bulk and grain boundary diffusion. Thus, if potassium would form a melt along the grain boundaries one would expect the diffusion to be accelerated. This can however not be concluded, from this study, as no Cl was detected in the analysis. Nevertheless, as mentioned above, Cl may have reacted and migrated after exposure why the explanation cannot be ruled out.

Cantatore et al. [38] investigated possible transport mechanisms for chlorine through the oxide bulk and proposed that chlorine ions may diffuse along the same diffusion channels as oxygen vacancies. Bean et al. [49] studied the stability of oxygen vacancies at MgO grain boundaries and related a higher segregation energy at the oxide grain boundaries to a higher concentration of oxygen vacancies, compared to the bulk material. Thus, if chloride ions diffuse through oxygen vacancy diffusion channels, it is possible that grain boundaries are even more favorable pathways for chlorine. However, if chlorine were to diffuse via potassium decorated grain boundaries one would expect traces of chlorine in the grain boundaries, possibly even in the form of KCl. However, as mentioned above, it is still possible that Cl have migrated from this region after exposure, during the cooling process.

Last, but not least, a factor worth discussing is the oxide scale cracking and delamination often observed on low-alloyed steel exposed to KCl(s) [15,34–37]. Larsson et al. [36] studied  $Fe_2.25Cr_1Mo$  in the presence of KCl(s)+HCl(g) and found that the oxide scale retained its integrity when HCl(g) was added to the exposure environment. No indications of potassium were observed in the outward-growing oxide formed on the oxide scale that preserved its integrity (in the presence of KCl(s)+HCl(g)) [36]. Thus, it may be speculated that the potassium integration is destructive in other ways than only by changing the diffusion properties, e.g. by inducing oxide delamination and crack formation. If potassium is part in widening the oxide grain boundary region, it is possible that this would simplify for crack propagation along the grain boundaries which in turn would result in lost integrity of the oxide scale. Note that this is only a speculation at this point.

The KCl-nanoclusters detected is intriguing and may be formed in several ways. One possibility is that small amounts of KCl on the surface gets trapped as the oxide grows. The clusters could in addition have been formed after exposure, during the cooling process, by reaction between K and Cl solved in the oxide scale at 400 °C. This may explain the absence of Cl in the oxide scale. However, it is very difficult to draw any conclusions regarding that from this study.



#### 4.4. Impact and outlook

The results observed in this study may give some insight into how small changes in the chemistry of an iron oxide scale could influence the overall growth rate of the oxide. An increased understanding of how potassium and chlorine may interplay to accelerate the corrosion of Fe-rich oxide scales may open up new ideas for ways to decrease corrosion in highly corrosive environments. The suggested accelerated grain boundary diffusion, possibly caused by potassium segregation, could also be of great interest for the development and implementation of predictive modeling tools for oxidation at relatively low temperatures (where grain boundary diffusion is often rate limiting). Thus, a better understanding of how grain boundary diffusion is altered in different exposure conditions could accelerate and greatly improve the development of lifetime predictive tools for oxidation, which in the future could reduce both material and maintenance costs.

#### 5. Conclusions

The results suggested that potassium is segregated to iron oxide grain boundaries in the outward-growing scale. It is proposed that the segregation of K in oxide grain boundaries is part in explaining the increased diffusion rate observed in the presence of KCl by enabling for other species, such as e.g. Cl, to diffuse faster to the oxide/metal interface. Chlorine, along with potassium, is also observed to be distributed in small ( $\leq 5$  nm) clusters throughout the top part of the outward-growing oxide, not related to the oxide grain boundaries.

#### CRedit authorship contribution statement

**Amanda Persdotter:** Conceptualization, Validation, Investigation, Data curation, Writing – original draft, Writing – review & editing, Visualization. **Torben Boll:** Investigation, Validation, Data curation, Writing – review & editing, Supervision, Project administration, Funding acquisition. **Torbjörn Jonsson:** Conceptualization, Validation, Writing – review & editing, Supervision, Project administration, Funding acquisition.

#### Declaration of Competing Interest

The authors declare that they have no known competing financial interests or personal relationships that could have appeared to influence the work reported in this paper.

#### Data Availability

The raw and processed data required to reproduce these findings cannot be shared at this time due to technical or time limitations.

#### Acknowledgments

This work was carried out within the Swedish High Temperature Corrosion Centre (HTC) at Chalmers University of Technology and the Karlsruhe nano micro facility (knmf, project 2019–021-025781), that are hereby gratefully acknowledged together with the Swedish Energy Agency and the member companies (AB Sandvik Materials Technology, Kanthal AB, Energiforsk AB, MH Engineering AB, Thermo-Calc Software AB, Valmet Technologies Oy, Sumitomo SHI FW Energia Oy, Babcock and Wilcox Volund A/S and MEC BioHeat and Power A/S). The research was performed in part at the Chalmers Materials Analysis Laboratory, CMAL, and also acknowledges M. Sattari at Chalmers university of technology for help with oxide grain imaging as well as E. Larsson and M. A. Olivás Ogaz for performing the furnace exposures.

#### References

- [1] N. Birks, G.H. Meier, F.S. Pettit, *Introduction to the High-temperature Oxidation of Metals*, Cambridge University Press, 2006.
- [2] D.J. Young, *High Temperature Oxidation and Corrosion of Metals*, Second edition., Elsevier, 2016.
- [3] D. Whittle, J. Stringer, Improvement in properties: additives in Oxidation Resistance. Improvements in high temperature oxidation resistance by additions of reactive elements or oxide dispersions, *Philos. Trans. R. Soc. Lond. A* 295 (VIII) (1980) 309–329.
- [4] J. Stringer, The reactive element effect in high-temperature corrosion, *Mater. Sci. Eng. A* 120–121 (PART 1) (1989) 129–137.
- [5] B.A. Pint, Progress in understanding the reactive element effect since the Whittle and Stringer literature review, *John String Symp. High. Temp. Corros.* (2001) 9–19.
- [6] D. Naumenko, B.A. Pint, W.J. Quadackers, Current thoughts on reactive element effects in alumina-forming systems: in memory of John Stringer, *Oxid. Met.* 86 (1–2) (2016) 1–43.
- [7] J. Jedlinski, General aspects of the reactive element effect, *Corros. Sci.* 35 (1993) 5–8.
- [8] K. Stiller, L. Viskari, G. Sundell, F. Liu, M. Thuvander, H.O. Andrén, D.J. Larson, T. Prosa, D. Reinhard, Atom probe tomography of oxide scales, *Oxid. Met.* 79 (3–4) (2013) 227–238.
- [9] Y. Chen, R.C. Reed, E.A. Marquis, Interfacial solute segregation in the thermally grown oxide of thermal barrier coating structures, *Oxid. Met.* 82 (5–6) (2014) 457–467.
- [10] K.A. Unocic, Y. Chen, D. Shin, B.A. Pint, and E.A. Marquis, STEM and APT characterization of scale formation on a La,Hf,Ti-doped NiCrAl model alloy, *Micron*, 109, April, 2018: 41–52. Available: (<https://doi.org/10.1016/j.micron.2018.01.011>).
- [11] D. Bramhoff, H.J. Grabke, E. Reese, H.P. Schmidt, Einfluß von HCl und Cl<sub>2</sub> auf die Hochtemperaturkorrosion des 2 1/4 Cr 1 Mo-Stahls in Atmosphären mit hohem Sauerstoffdrücken, *Mater. Corros.* 41 (6) (1990) 303–307.
- [12] E. Reese, H.J. Grabke, Einfluß von Chloriden auf die Oxidation, *Werkst. und Korros.* 43 (1992) 547–557.
- [13] H.J. Grabke, E. Reese, M. Spiegel, The effects of chlorides, hydrogen-chloride, and sulfur-dioxide in the oxidation of steels below deposits, *Corros. Sci.* 37 (7) (1995) 1023–1043.
- [14] A. Zahr, M. Spiegel, H.J. Grabke, The influence of alloying elements on the chlorine-induced high temperature corrosion of Fe-Cr alloys in oxidizing atmospheres, *Mater. Corros.* 50 (10) (1999) 561–578.
- [15] Y.S. Li, Y. Niu, W.T. Wu, Accelerated corrosion of pure Fe, Ni, Cr and several Fe-based alloys induced by ZnCl<sub>2</sub>-KCl at 450°C in oxidizing environment, *Mater. Sci. Eng. A* 345 (2003) 64–71.
- [16] A. Zahr, M. Spiegel, H.J. Grabke, Chloridation and oxidation of iron, chromium, nickel and their alloys in chloridizing and oxidizing atmospheres at 400–700 °C, *Corros. Sci.* 42 (6) (2000) 1093–1122.
- [17] F. Wang, Y. Shu, Influence of Cr content on the corrosion of Fe-Cr alloys: the synergistic effect of NaCl and water vapor, *Oxid. Met.* 59 (3–4) (2003) 201–214.
- [18] M. Spiegel, A. Zahr, H.J. Grabke, Fundamental aspects of chlorine induced corrosion in power plants, *Mater. High. Temp.* 20 (2) (2003) 153–159.
- [19] M.A. Uusitalo, P.M.J. Vuoristo, T.A. Mantyla, High temperature corrosion of coatings and boiler steels in oxidizing chlorine-containing atmosphere, *Mater. Sci. Eng. a-Struct. Mater. Prop. Microstruct. Process.* 346 (1–2) (2003) 168–177.
- [20] S. Sroda, S. Tuurna, K. Penttilä, and L. Heikinheimo, High Temperature Oxidation Behaviour of Boiler Steels under Simulated Combustion Gases, *Materials Science Forum*, 461–464, 2004: 981–988. Available: (<http://www.scientific.net/MSF.461-464.981>).
- [21] M.A. Uusitalo, P.M.J. Vuoristo, T.A. Mantyla, High temperature corrosion of coatings and boiler steels below chlorine-containing salt deposits, *Corros. Sci.* 46 (6) (2004) 1311–1331.
- [22] J. Pettersson, H. Asteman, J.E. Svensson, L.G. Johansson, KCl induced corrosion of a 304-type austenitic stainless steel at 600 degrees C; the role of potassium, *Oxid. Met.* 64 (1–2) (2005) 23–41.
- [23] J. Pettersson, J.E. Svensson, L.G. Johansson, Alkali induced corrosion of 304-type austenitic stainless steel at 600 degrees C; comparison between KCl, K<sub>2</sub>CO<sub>3</sub> and K<sub>2</sub>SO<sub>4</sub>, *Mater. Sci. Forum* 595–598 (2008) 367–375.
- [24] C. Pettersson, L.G. Johansson, J.E. Svensson, The influence of small amounts of KCl (s) on the initial stages of the corrosion of alloy Sanicro 28 at 600 degrees C, *Oxid. Met.* 70 (5–6) (2008) 241–256.
- [25] C. Proff, T. Jonsson, C. Pettersson, J.E. Svensson, L.G. Johansson, M. Halvarsson, Microstructural investigation of the KCl-induced corrosion of the austenitic alloy Sanicro 28 (35Fe27Cr31Ni) at 600°C, *Mater. High. Temp.* 26 (2) (2009) 113–125.
- [26] S. Karlsson, J. Liske, L.-G. Johansson, J.-E. Svensson, Alkali induced high temperature corrosion of stainless steel: the influence of NaCl, KCl and CaCl<sub>2</sub>, *Oxid. Met.* 78 (2012) 83–102.
- [27] S.C. Cha, M. Spiegel, Local reactions of KCl particles with iron, nickel and chromium surfaces, *Mater. Corros.* 57 (2) (2006) 159–164.
- [28] S. Sroda, S. Tuurna, Laboratory scale tests on corrosion behavior of boiler materials in simulated combustion atmospheres (EU Project - OPTICORR), *Mater. Corros.* 57 (3) (2006) 244–251.
- [29] N. Folkeson, L.G. Johansson, J.E. Svensson, Initial stages of the HCl-induced high-temperature corrosion of alloy 310, *J. Electrochem. Soc.* 154 (9) (2007) C515–C521.

- [30] H.T. Ma, C.H. Zhou, L. Wang, High temperature corrosion of pure Fe, Cr and Fe-Cr binary alloys in O<sub>2</sub> containing trace KCl vapour at 750 degrees C, *Corros. Sci.* 51 (8) (2009) 1861–1867.
- [31] T. Jonsson, J. Froitzheim, J. Pettersson, J.E. Svensson, L.G. Johansson, M. Halvarsson, The influence of KCl on the corrosion of an Austenitic stainless steel (304L) in oxidizing humid conditions at 600°C: A microstructural study, *Oxid. Met.* 72 (3–4) (2009) 213–239.
- [32] J. Sui, J. Lehmusto, M. Bergelin, H. Mikko, The Effects of KCl, NaCl and K<sub>2</sub>CO<sub>3</sub> on the high-temperature oxidation onset of sanicro 28 steel, *Oxid. Met.* 85 (2016) 565–598.
- [33] A.M. Olivas-Ogaz, J. Eklund, A. Persdotter, M. Sattari, J. Liske, J.-E. Svensson, and T. Jonsson, The Influence of Oxide-Scale Microstructure on KCl(s)-Induced Corrosion of Low-Alloyed Steel at 400°C, *Oxidation of Metals*, 0123456789, 2018.
- [34] T. Jonsson, N. Folkesson, J.-E. Svensson, L.-G. Johansson, M. Halvarsson, An ESEM in situ investigation of initial stages of the KCl induced high temperature corrosion of a Fe-2.25Cr-1Mo steel at 400°C, *Corros. Sci.* 53 (2011) 2233–2246.
- [35] N. Folkesson, T. Jonsson, M. Halvarsson, L.G. Johansson, J.E. Svensson, The influence of small amounts of KCl(s) on the high temperature corrosion of a Fe-2.25Cr-1Mo steel at 400 and 500°C, *Mater. Corros.* 62 (7) (2011) 606–615.
- [36] E. Larsson, J. Liske, A. Persdotter, T. Jonsson, J.E. Svensson, and L.G. Johansson, The Influence of KCl and HCl on the High-Temperature Oxidation of a Fe-2.25Cr-1Mo Steel at 400°C, *Oxidation of Metals*, 93, 1–2, 2020: 29–52. Available: (<https://doi.org/10.1007/s11085-019-09943-9>).
- [37] A. Persdotter, M. Sattari, E. Larsson, M.A. Olivas Ogaz, J. Liske, and T. Jonsson, Oxidation of Fe-2.25Cr-1Mo in presence of KCl(s) at 400°C - Crack formation and its influence on oxidation kinetics, *Corrosion Science*, 163, 2020: 108234. Available: (<https://doi.org/10.1016/j.corsci.2019.108234>).
- [38] V. Cantatore, M.A. Olivas Ogaz, J. Liske, T. Jonsson, J.E. Svensson, L.G. Johansson, I. Panas, Oxidation driven permeation of iron oxide scales by chloride from experiment guided first-principles modeling, *J. Phys. Chem. C* 123 (42) (2019) 25957–25966.
- [39] M.J. McNallan, W.W. Liang, S.H. Kim, C.T. Kang, Acceleration of the oxidation of metals by chlorine, *High. Temp. Corros., NACE* (1983) 316–321.
- [40] H.P. Nielsen, F.J. Frandsen, K. Dam-Johansen, L.L. Baxter, Implications of chlorine-associated corrosion on the operation of biomass-fired boilers, *Prog. Energy Combust. Sci.* 26 (3) (2000) 283–298.
- [41] M. Montgomery, A. Karlsson, O.H. Larsen, Field test corrosion experiments in Denmark with biomass fuels Part 1: straw-firing, *Mater. Corros. -Werkst. Und Korros.* 53 (2) (2002) 121–131.
- [42] F.J. Frandsen, Utilizing biomass and waste for power production – a decade of contributing to the understanding, interpretation and analysis of deposits and corrosion products, *Fuel* 84 (10) (2005) 1277–1294.
- [43] P. Henderson, P. Szakalos, R. Pettersson, C. Andersson, J. Hogberg, Reducing superheater corrosion in wood-fired boilers, *Mater. Corros.* 57 (2) (2006) 128–134.
- [44] N. Mortazavi, C. Geers, M. Esmaily, V. Babic, M. Sattari, K. Lindgren, P. Malmberg, B. Jönsson, M. Halvarsson, J.E. Svensson, I. Panas, and L.G. Johansson, Interplay of water and reactive elements in oxidation of alumina-forming alloys, *Nature Materials*, 17, 7, 2018: 610–617. Available: (<https://doi.org/10.1038/s41563-018-0105-6>).
- [45] M.A. Olivas-Ogaz, J. Eklund, J.E. Svensson, J. Liske, T. Jonsson, Microstructural study of the influence of KCl and HCl on preformed corrosion product layers on stainless steel, *Oxid. Met.* 87 (5–6) (2017) 801–811.
- [46] J.A.V. Orman, K.L. Crispin, Diffusion in oxides, *Rev. Mineral. Geochem.* 72 (2010) 757–825.
- [47] P. Deng, Q. Peng, and E.H. Han, Grain boundary oxidation of proton-irradiated nuclear grade stainless steel in simulated primary water of pressurized water reactor, *Scientific Reports*, 11, 1, 2021: 1–9. Available: (<https://doi.org/10.1038/s41598-020-80600-x>).
- [48] I. Kaur, W. Gust, *Fundamentals of Grain and Interface Boundary Diffusion*, Ziegler Press, Stuttgart, 1989.
- [49] J.J. Bean, K.P. McKenna, Stability of point defects near MgO grain boundaries in FeCoB/MgO/FeCoB magnetic tunnel junctions, *Phys. Rev. Mater.* 2 (12) (2018).
- [50] K. Yagi, Creep Properties of Heat Resistant Steels and Superalloys · 2.25Cr-1Mo steel, in *Creep Properties of Heat Resistant Steels and Superalloys*, Group VIII Advanced Materials and Technologies, Volume 2B, H. W. K. Yagi, G. Merckling, T.-U. Kern, H. Irie, Ed. SpringerMaterials, 2004: 67.